Organic Electronics 14 (2013) 451–456

Contents lists available at SciVerse ScienceDirect

Organic Electronics

journal homepage: www.elsevier.com/locate/orgel

Highly ordered C_{60} films on epitaxial Fe/MgO(001) surfaces for organic spintronics

P.K.J. Wong [a,1], T.L.A. Tran [a,1], P. Brinks [b], W.G. van der Wiel [a], M. Huijben [b], M.P. de Jong [a,*]

[a] NanoElectronics Group, MESA+ Institute for Nanotechnology, University of Twente, P.O. Box 217, Enschede 7500 AE, The Netherlands
[b] Faculty of Science and Technology, MESA+ Institute for Nanotechnology, University of Twente, P.O. Box 217, Enschede 7500 AE, The Netherlands

ARTICLE INFO

Article history:
Received 5 October 2012
Received in revised form 26 November 2012
Accepted 26 November 2012
Available online 22 December 2012

Keywords:
Fullerenes
Organic spintronics
X-ray diffraction
Scanning tunneling microscopy

ABSTRACT

Hybrid interfaces between ferromagnetic surfaces and carbon-based molecules play an important role in organic spintronics. The fabrication of devices with well defined interfaces remains challenging, however, hampering microscopic understanding of their operation mechanisms. We have studied the crystallinity and molecular ordering of C_{60} films on epitaxial Fe/MgO(001) surfaces, using X-ray diffraction and scanning tunneling microscopy (STM). Both techniques confirm that fcc molecular C_{60} films with a (111)-texture can be fabricated on epitaxial bcc-Fe(001) surfaces at elevated growth temperatures (100–130 °C). STM measurements show that C_{60} monolayers deposited at 130 °C are highly ordered, exhibiting quasi-hexagonal arrangements on the Fe(001) surface oriented along the [100] and [010] directions. The mismatch between the surface lattice of the monolayer and the bulk fcc C_{60} lattice prevents epitaxial overgrowth of multilayers.

1. Introduction

Hybrid ferromagnet (FM)/organic interfaces have become a subject of intensive research since the last decade, as fueled by observations of strong magnetoresistance (MR) effects in FM/organic spin-valves [1–4]. This has sparked the development of a new research field, which has been coined "organic spintronics", aiming to (i) establish additional functionality in organic electronic devices via active use of charge carrier spins, or (ii) to incorporate organic materials into spintronic devices.

The central motivation for utilizing organic semiconductors as hosts for spin polarized charge carriers relies on their weaker spin–orbit coupling and hyperfine interaction as compared to inorganic semiconductors. This holds great promise for attaining long spin lifetimes, offering prospects for robust spin manipulation and readout in organic spintronic devices [5,6]. It is noteworthy, however, that many of the previously examined spin-valve structures featured ill-defined FM/organic interfaces, and failed to offer a reliable picture of the physical mechanisms behind the spin-dependent effects. In order to harness the full potential of this infant yet promising field, systematic investigations of the effects of structural, electronic, and magnetic properties of the FM/organic interfaces on spin injection, transport and extraction are very important. The incorporation of well-characterized and structurally ordered hybrid interfaces into devices would allow for a direct comparison with theoretical modeling, making spin transport studies much more informative, and therefore paving the way to the understanding of novel spin physics involved at the heterojunctions.

Interfaces comprised of C_{60} and bcc-Fe(001) form interesting model systems for organic spintronics, because of the following reasons. (1) Bcc-Fe(001) features fully spin-polarized Δ_1-electrons, which produces very high tunneling MR when combined with a crystalline MgO tunnel barrier [7]. It is interesting to investigate whether similar effects can be exploited at structurally ordered Fe/organic interfaces. (2) C_{60} lacks hydrogen and the

* Corresponding author.
E-mail address: m.p.dejong@utwente.nl (M.P. de Jong).
[1] These authors contributed equally.

1566-1199/$ - see front matter © 2012 Elsevier B.V. All rights reserved.
http://dx.doi.org/10.1016/j.orgel.2012.11.034

associated spin dephasing mechanism by hyperfine coupling (the predominantly present ^{12}C isotopes have zero nuclear spin). (3) The high electron affinity of C_{60} (of about 4 eV) [8] results in small energy barriers for electron injection at the interfaces with 3*d* transition metal FMs, such that devices can be operated at low bias, which is beneficial for attaining a high spin polarization of the injected current. (4) Finally, C_{60} molecules have been observed to form well-ordered (and in some cases even epitaxial) layers on a variety of surfaces as we will address below, due to the non-stringent requirements for surface energy- and lattice matching typical for organic semiconductors. In contrast to inorganic materials, epitaxial and well-ordered growth of organic semiconductors therefore might be achieved even on lattice-mismatched substrates. Our previous studies on the electronic and magnetic properties of C_{60}/bcc-Fe(001) interfaces, using synchrotron-based core-level electron spectroscopies, revealed significant hybridization between the π-electronic states of C_{60} and the 3*d*-bands of the Fe surface, which induces a strong magnetic polarization of C_{60}-derived electronic orbitals [9]. The presence of such spin-dependent hybridization is critical, since it is expected to play a decisive role in spin transport across the hybrid interface [3]. Moreover, the strong interfacial interaction will certainly exert a non-trivial impact on the growth mechanism and structural properties of C_{60} overlayers on Fe(001) surfaces, as is also the case for C_{60} on Al [10], Cu [11], and Ni surfaces [12]. This particularly interesting aspect forms the core of the present work. Using a combinatorial approach of X-ray diffraction (XRD) and scanning tunneling microscopy (STM), we give insight into the crystallinity and local structural ordering of C_{60} molecules, that could be accomplished atop epitaxial bcc-Fe(001) films on MgO(001) for organic spintronic applications.

2. Experimental methods

Our C_{60}/Fe bilayer films were prepared onto single-crystalline MgO(001) substrates in a UHV molecular-beam epitaxy system with a base pressure of 10^{-10} mbar. The commercial MgO(001) substrates used in this experiment exhibited a root mean square roughness of about 0.15 nm. Prior to any *in situ* treatment, the substrates were ultrasonically cleaned thoroughly in acetone, ethanol and isopropanol at 50 °C. While in UHV, the substrates were thermally annealed at 450 °C for 60 min to obtain clean surfaces, on top of which a 10-nm thick epitaxial Fe(001) film was grown by e-beam evaporation at a rate of 0.9 nm/min at an elevated substrate temperature of 150 °C. C_{60} multilayers with a thickness of about 100-nm were then deposited onto the Fe(001) by thermal evaporation from a Knudsen-cell (operated at 500 °C) at a rate of 3.3 nm/min and with a substrate temperature of 100 °C. The crystallinity and structural properties of these so-fabricated film stacks were characterized *ex situ* by XRD. The XRD measurements were carried out with a Bruker AXS D8 DISCOVER diffractometer using Cu Kα radiation (wavelength: 0.154 nm) equipped with a four-circle goniometer.

To investigate the adsorption mechanism and local structural ordering of C_{60} on the epitaxial Fe(001) surface down to the molecular scale, we used a commercial UHV–STM with an interconnected custom-made sample preparation chamber. C_{60}/Fe/MgO(001) samples were prepared under similar experimental conditions as described above. In order to obtain reliable electrical contacts between the deposited films and the sample holder, two 30-nm thick W strips were sputtered *ex situ* on both edges of the insulating MgO substrates using a dedicated DC-sputtering tool. These strips were found to be very stable against any thermal (cleaning) treatments, without causing any detectable diffusion of W atoms across the surface. STM images were acquired in constant current mode using mechanically cut Pt–Ir tips at room temperature (RT) with a set-point current of 0.8 nA and a bias voltage of 230 mV.

3. Results and discussion

3.1. Structural characterization by X-ray diffraction

Fig. 1a shows a XRD θ–2θ scan of a 100 nm C_{60}/10 nm Fe/MgO(001) sample, from which the diffraction peaks of fcc-C_{60} (111), (222) and (333), bcc-Fe (002), and MgO (002), as labelled, are clearly observed. When compared to the powder diffraction pattern of C_{60} [3] and XRD measurements of C_{60} films on other metal substrates, [13] the existence of only (*hhh*) diffraction peaks from our C_{60} film indicates a fcc-(111) texture. Fig. 1b–d shows the ω scans, or rocking curves, of the MgO(002), Fe(002), and C_{60}(111) diffraction peaks, respectively. We fitted each rocking curve with a Gaussian function in order to extract the full-width at half maximum (FWHM), a parameter that quantifies the crystallinity along the film normal. A small FWHM value of 0.03° for MgO(002) peak confirms the high crystallinity of the MgO(001) substrates we used in this study, while the FWHM values for Fe(002) and C_{60}(111) are larger, 1.56° and 2.51°, due to the lower thickness and higher defect density of the deposited layers. We will elaborate this specific point in later paragraphs. Interestingly, the C_{60}(111) rocking curve in Fig. 1d exhibits two parts: a sharp narrow peak superimposed on a much broader peak, which is characteristic for weakly disordered systems [14]. The lattice mismatch between the C_{60} layer and the Fe/MgO stack underneath (see further discussion below) results in the formation of dislocations. The non-uniformity of the strains concentrated at the dislocation gives rise to diffuse scattering. When the dislocation density is large, the diffraction peak from the C_{60} layer is broadened, due to short-range correlations in positions of the atoms. The intensity of the narrow coherent peak, reflecting the long-range correlations, is small. The φ-scans of the same sample in Fig. 1e, which probe the in-plane lattice matching of substrate and adlayers, reveal an epitaxial relationship between the MgO substrate and the Fe layer. As shown, the in-plane signals corresponding to the Fe epitaxial film are always 45° off from those detected from the MgO(001) substrate, which is in good agreement with the previously reported epitaxial relationship of Fe(001)[100]//MgO(001)[110] [15]. However, no diffraction peaks containing an in-plane component could be detected for the (100 nm thick) C_{60} layer, indicating the

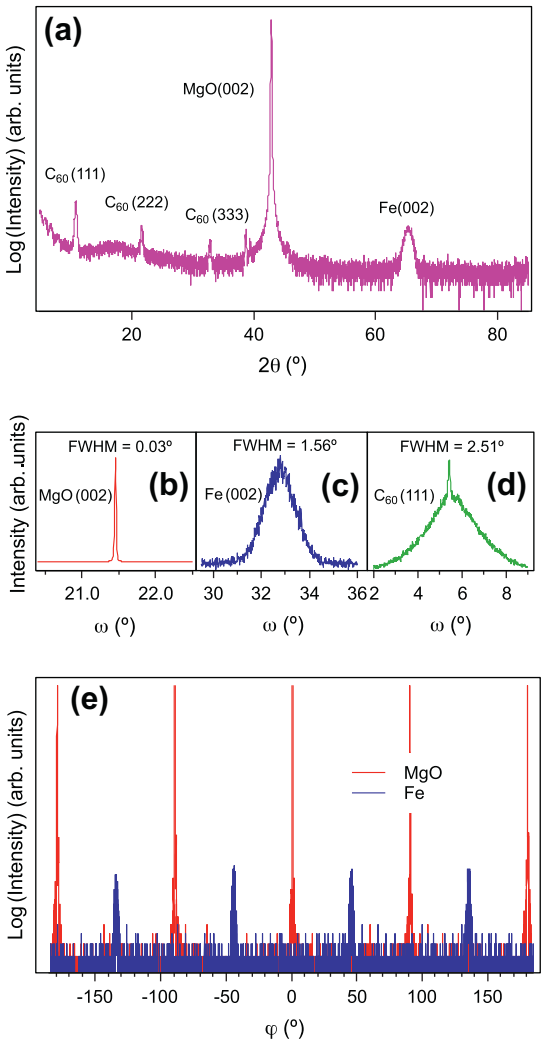

Fig. 1. XRD measurements of 100-nm C_{60}/10-nm Fe/MgO(001). (a) Wide-angle θ–2θ scan; (b–d) ω-scans or rocking curves for MgO(002), Fe(002) and C_{60}(111) diffraction peaks; (e) φ-scan for MgO(022) and C_{60}-capped Fe(022) peaks.

absence of an in-plane structural relationship between the C_{60} layer and the Fe/MgO stack underneath. This suggests either a complete in-plane disorder, or the presence of only short-range molecular order in the plane of the C_{60} film. Given that the sensitivity of XRD for the interface region is limited, however, some degree of in-plane ordering may be present for ultrathin films. We will address this issue next using STM measurements.

3.2. Surface morphology and molecular ordering by scanning tunneling microscopy

Fig. 2 shows a series of STM images, capturing the surface morphology at different stages of C_{60} monolayer (ML) fabrication by thermal desorption of its multilayers (deposited at RT) on an Fe(001) surface. Similar procedures have been adopted and described in our previous report on the electronic/magnetic structure at the ML C_{60}/Fe(001) interface [9]. Fig. 2a depicts an STM image of a 10-nm thick Fe(001) film epitaxially grown on a clean MgO(001) surface at 150 °C. Previous studies have shown that two-dimensional growth of bcc-Fe on MgO(001) is only possible at or above a critical temperature such that the Schwöbel barrier for downward step diffusion can be overcome [16,17]. Indeed, the observation of an atomically flat Fe film surface, with well-defined terraces and step structures that align along the Fe[100] or MgO[110] crystallographic directions confirms this thermodynamic growth process, and also serves as evidence for high-quality epitaxial growth. The pits observed in the film are due to screw dislocations, which are structural defects that result from the lattice mismatch of 3.8% between bcc-Fe and the (45° rotated) rock-salt structure of MgO(001). Although larger Fe terraces could be obtained using a higher growth temperature than that used in this present experiment, as revealed by our AFM measurements (not shown), the resulting films consisted of many discontinuous Fe terraces, hampering any STM measurement due to poor electrical conductivity. Fig. 2b illustrates the sample morphology with a C_{60} multilayer on top of the Fe surface. The C_{60} deposition at RT essentially washes out the atomic step structures of the Fe film, although the deep pits due to screw dislocations remain discernable. The high density of voids also suggests that the C_{60} growth proceeded with a three-dimensional island-growth mode. At this point, we conclude that no structural ordering of the C_{60} film exists, and that the multilayer can thus be described as amorphous-like. With a brief anneal at 280 °C for 3 min, a substantial part of the C_{60} molecules appear to have been desorbed from the surface, judging from the partial recovery of the Fe surface morphology (Fig. 2c). This is in good agreement with our X-ray absorption spectroscopy data in Ref. [10], which shows that annealing at or above 280 °C results in desorption of C_{60} overlayers, while a ML of chemisorbed C_{60} molecules is retained at the surface. These molecules are bound by the strong interaction with the underlying Fe layer, which is apparent from the hybridization-induced modifications of the C_{60} π^*-orbitals [9]. A close-up image of the annealed film, Fig. 2d, reveals that the residual C_{60} molecules remain largely disordered. Fig. 2e and f shows the same surface after an additional 3 min of annealing at the same temperature. Now, short-ranged ordered areas can be observed, such as those marked with blue arrows in Fig. 2f, embedded in a still largely disordered environment.

Next, we consider the case of a (partial) C_{60} monolayer obtained by adsorbing molecules onto a hot Fe(001) surface. Dosing C_{60} molecules onto substrates held at elevated temperatures is known to result in the growth of highly ordered monolayer films on various metal substrates that feature different interaction strengths with C_{60} [10–12,18,19]. Depending on the nature of the interfacial interaction, the adsorbed molecules may require a higher thermal energy to attain an equilibrium arrangement on a given substrate surface, which defines a temperature window within which growth of highly ordered MLs may be realized. Fig. 3a and b shows molecular resolution STM images of a C_{60} ML on Fe(001) grown at a deposition

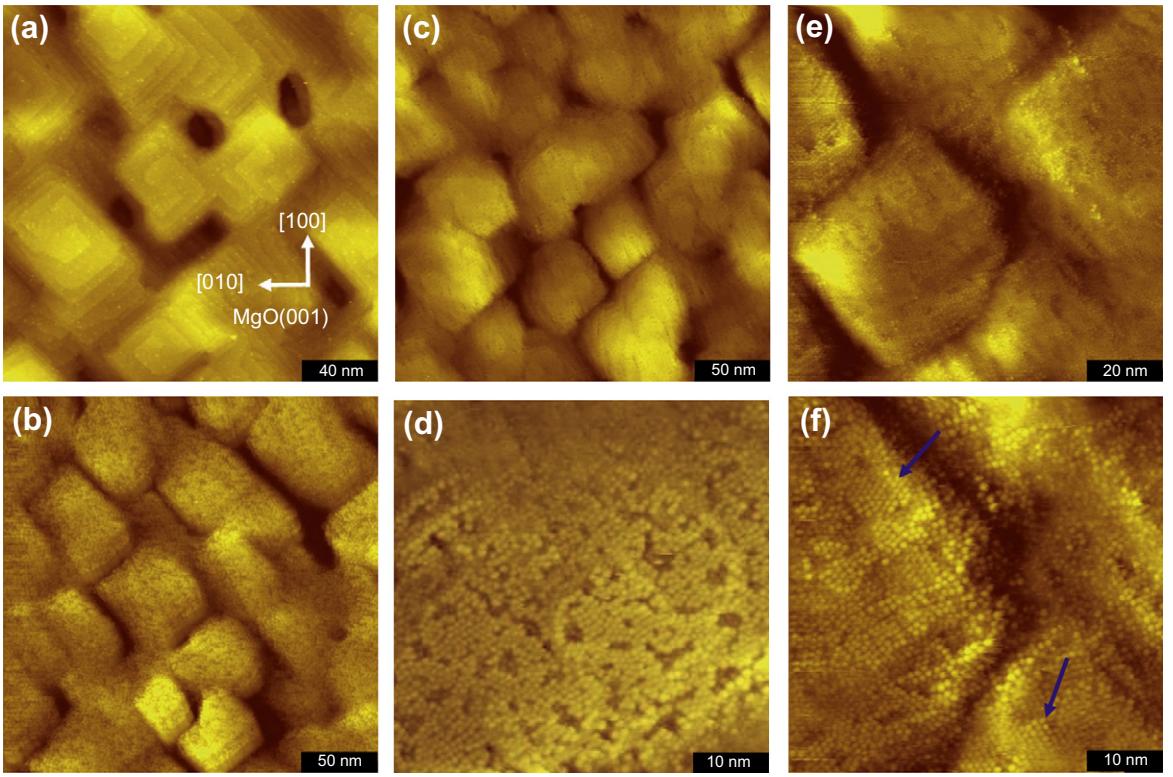

Fig. 2. Surface morphology of C_{60}/10-nm Fe/MgO(001) acquired by STM at RT. (a) Epitaxial Fe(001) surface grown on MgO(001). The arrows show the crystallographic directions of the MgO(001) substrate; (b) after C_{60} multilayer deposition at RT; (c) after annealing at 280 °C for 3 min; (d) molecular resolution image of (c); (e) after further annealing at 280 °C for 3 min; (f) molecular resolution image of (e). The blue arrows indicate areas where (short-range) C_{60} molecular ordering can be seen. (For interpretation of the references to color in this figure legend, the reader is referred to the web version of this article.)

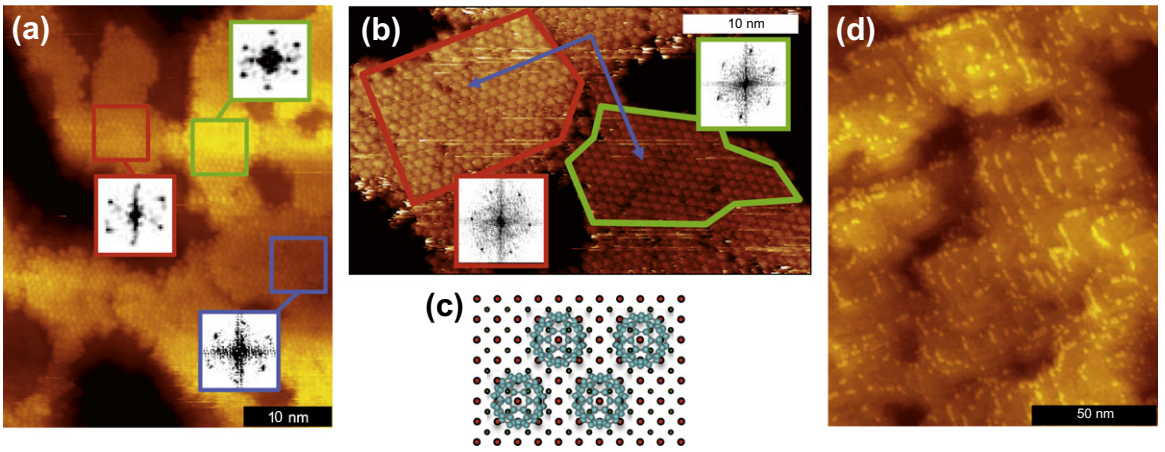

Fig. 3. (a) Surface morphology of a ML of C_{60} on 10-nm Fe/MgO(001) with C_{60} deposited at a substrate temperature of 130 °C. The insets show FFT images of selected areas as marked by contours; (b) another area of the same sample as in (a) where different orientations of the C_{60} surface structure on Fe(001) are observed, rotated by 90° relative to each other. The blue arrows indicate the Fe [100] and [010] directions, the insets show FFT images of the areas enclosed by the red/green contours; (c) proposed surface structure of the C_{60} ML on Fe(001). Red (blue) dots indicate the positions of the Fe atoms in the first (second) layer of the bcc surface; (d) Surface structure of a sub-ML C_{60} on 10-nm Fe/MgO(001), where atomic steps are preferentially occupied by C_{60}, forming chains of molecules. (For interpretation of the references to color in this figure legend, the reader is referred to the web version of this article.)

temperature of 130 °C (comparable to the growth temperature of the 100 nm C_{60} film that was analyzed with XRD). Fast Fourier transform (FFT) images for several selected areas, marked by contours, are shown as insets in Fig. 3a and b. The STM images and their FFTs clearly reveal that the ML is highly ordered, and that the C_{60} molecules are

packed in a quasi-hexagonal arrangement. Intermolecular distances determined from the various STM images that we recorded are consistently close to 1 nm, while the slightly asymmetric FFT spot patterns indicate a periodic structure consisting of distorted hexagons, with aspect ratios of 1.1 for the long/short diagonals connecting the corner points. Two distinct orientations of the C_{60} adsorbate lattice on the Fe(001) surface could be observed, rotated by 90°, such as those shown within the red and green contours in Fig. 3b containing rows of molecules that are either along the Fe[100] or [010] directions (indicated by the blue arrows). These findings are consistent with the proposed structure shown in Fig. 3c, comprising C_{60} molecules in equivalent adsorption sites on the Fe(001) surface. The description of the unit cell of this quasi-hexagonal overlayer structure requires matrix notation:

$$\begin{pmatrix} \vec{b}_1 \\ \vec{b}_2 \end{pmatrix} = \begin{pmatrix} 4 & 0 \\ 2 & 3 \end{pmatrix} \begin{pmatrix} \vec{a}_1 \\ \vec{a}_2 \end{pmatrix},$$

where $\vec{a}_1$, $\vec{a}_2$ and $\vec{b}_1$, $\vec{b}_2$ are the unit cell vectors of the Fe and C_{60} lattices, respectively. Taking the Fe lattice constant to be 0.287 nm, the lengths of the C_{60} unit cell vectors are 1.148 nm and 1.035 nm, implying an aspect ratio 1.109 of the distorted hexagonal lattice, in good agreement with the experiments. The length of the shorter unit cell vector is very close to the intermolecular distance of 1.002 nm in the (111) planes of the fcc lattice of bulk C_{60} (which has a lattice constant of 1.417 nm), while the length of the longer unit cell vector deviates by more than 10%.

We propose that the lattice mismatch between the first ML of C_{60} on Fe(001) and the bulk structure is a primary cause for the absence of a well-defined in-plane ordering in multilayer films. Sakurai et al. reported that epitaxial C_{60} films can be obtained on lattice-mismatched substrates such as MoS_2 [20], due to the weak Van der Waals-type interfacial interaction, such that C_{60} molecules can arrange themselves incommensurate with the MoS_2 lattice. On the contrary, for systems featuring a strong interaction, such as in the present case or, for example, C_{60} on Ni(110) [15], a good lattice match becomes a prerequisite for epitaxial growth. It should be noted that strong chemical interactions, involving spin polarized hybrid orbitals, typically occur at interfaces between transition metal ferromagnets and π-conjugated carbon systems [3,9,21–23]. A further complication is the non-negligible disorder that is observed in the STM images of the ML C_{60} films (see Fig. 3).

By examining the adsorption mechanism and molecular arrangement of C_{60} at the sub-ML regime, we conclude that atomic step structures on the Fe(001) surface may partly account for this disorder. It is shown in Fig. 3d that the most probable sites for C_{60} nucleation are atomic steps, where the adsorbed molecules form chains in parallel to those of the edges. Such initial nucleation has been similarly observed on Bi(001)/Si(111), where a high density of screw dislocations is also present [24]. Diffusing adatoms or molecules, which encounter a step can either be reflected at the step or cross the step. In the latter situation, they can then either continue diffusing or adsorb at the step edge. For C_{60} on Fe/MgO(001), adsorption of impinging molecules at the steps is efficient, as supported by Fig. 3d. At higher coverages, we expect that the steps will firstly be saturated before the molecules occupy the flat terraces, which may hamper the formation of highly ordered structures on these terraces.

4. Conclusions

Using XRD and STM, we have investigated the structural properties and local molecular ordering of C_{60} grown on epitaxial Fe/MgO(001). XRD analysis of 100 nm thick C_{60} molecular films shows that a strong (111) texture is obtained when growth is carried out at elevated temperature (100 °C). No long-range in-plane structural order could be detected in these 100 nm thick films. In contrast, STM measurements show that C_{60} forms a highly ordered monolayer on Fe(001). The molecules are arranged in a quasi-hexagonal pattern that superficially resembles the (111) plane of bulk fcc C_{60} but shows a considerable lattice mismatch with that structure. Most probably, this mismatch prevents epitaxial overgrowth of C_{60} films, consistent with our XRD measurements. It should be pointed out, however, that the in-plane structural order might persist for ultrathin films.

The (spin-dependent) electronic hybridization effects that we have observed previously for interfaces between C_{60} and Fe(001) result in strong interfacial interactions, which in turn have a profound impact on the growth mechanism in this hybrid system. Furthermore, STM measurements of MLs prepared under different conditions underline the important role of the kinetics of the adsorbed C_{60} molecules on the Fe surface in defining the structural properties of the first layer. The highly ordered surface structures are interesting within the context of spin polarization charge transport across the interface, since the well-defined molecular arrangement allows for direct comparison with theory. We expect that spin transport experiments on systems involving C_{60}/Fe(001) interfaces, and/or similarly well-defined and well-characterized interfaces, will generate important information for the further development of organic spintronic devices.

Acknowledgments

This work is funded by the European Research Council (ERC Starting Grant Nos. 280020 and 240433), and the NWO VIDI program (Grant No. 10246).

References

[1] Z.H. Xiong, D. Wu, Z.V. Vardeny, J. Shi, Nature 427 (2004) 821.
[2] T.S. Santos, J.S. Lee, P. Migdal, I.C. Lekshmi, B. Satpati, J.S. Moodera, Phys. Rev. Lett. 98 (2007) 016601.
[3] C. Barraud, P. Seneor, R. Mattana, S. Fusil, K. Bouzehouane, C. Deranlot, P. Graziosi, L. Hueso, I. Bergenti, V. Dediu, F. Petroff, A. Fert, Nat. Phys. 6 (2010) 615–620.
[4] V. Dediu, L.E. Hueso, I. Bergenti, A. Riminucci, F. Borgatti, P. Graziosi, C. Newby, F. Casoli, M.P. de Jong, C. Taliani, Y. Zhan, Phys. Rev. B 78 (2008) 115203.
[5] W.J.M. Naber, S. Faez, W.G. van der Wiel, J. Phys. D 40 (2007) R205.
[6] V.A. Dediu, L.E. Hueso, I. Bergenti, C. Taliani, Nat Mater. 8 (2009) 707.
[7] S. Yuasa, T. Nagahama, A. Fukushima, Y. Suzuki, K. Ando, Nat. Mater. 3 (2004) 868.
[8] P. Rudolf, M.S. Golden, P.A. Brühwiler, J. Electron Spectrosc. Relat. Phenom. 100 (1999) 409.

[9] T.L.A. Tran, P.K.J. Wong, M.P. de Jong, W.G. van der Wiel, Y.Q. Zhan, M. Fahlman, Appl. Phys. Lett. 98 (2011) 222505.
[10] A.J. Maxwell, P.A. Brühwiler, D. Arvanitis, J. Hasselström, M.K.-J. Johansson, N. Mårtensson, Phys. Rev. B 57 (1998) 7312.
[11] M. Abel, A. Dmitriev, R. Fasel, N. Lin, J.V. Barth, K. Kern, Phys. Rev. B 67 (2003) 245407.
[12] C.H. Lin, K.C. Lin, T.B. Tang, W.W. Pai, J. Nanosci. Nanotechno. 8 (2008) 602.
[13] J.G. Hou, J. Zeng, Y.Q. Li, Z.Q. Wu, Thin Solid Films 320 (1998) 179.
[14] V.M. Kaganer, R. Köhler, M. Schmidbauer, R. Opitz, B. Jenichen, Phys. Rev. B 55 (1997) 1793.
[15] C.M. Boubeta, J.L. Costa-Kramer, A. Cebollada, J. Phys. Condens. Mater. 15 (2003) R1123.
[16] J.F. Lawler, R. Schad, S. Jordan, H. van Kempen, J. Magn. Mater. 165 (1997) 224.
[17] B. Wassermann, Phil. Mag. 83 (2003) 1929.
[18] M.R.C. Hunt, S. Modesti, R. Rudolf, R.E. Palmer, Phys. Rev. B 51 (1995) 10039.
[19] J.K. Gimzewski, S. Modesti, R.R. Schlittler, Phys. Rev. Lett. 72 (1994) 1036.
[20] M. Sakurai, H. Tada, K. Koma, Jpn. J. Appl. Phys. 30 (1991) L1892.
[21] S. Javaid, M. Bowen, S. Boukari, L. Joly, J.B. Beaufrand, X. Chen, Y.J. Dappe, F. Scheurer, J.P. Kappler, J. Arabski, W. Wulfhekel, M. Alouani, E. Beaurepaire, Phys. Rev. Lett. 105 (2010) 077201.
[22] N. Atodiresei, J. Brede, P. Lazic, V. Caciuc, G. Hoffmann, R. Wiesendanger, S. Blugel, Phys. Rev. Lett. 105 (2010) 066601.
[23] M. Wesser, Y. Rehder, K. Horn, M. Sicot, M. Fonin, A.B. Preobrajenski, Appl. Phys. Lett. 96 (2010) 012504.
[24] J.T. Sadowski, R.Z. Bakhtizin, A.I. Oreshkin, T. Nishihara, A. Al-Mahboob, Y. Fujikawa, K. Nakajima, T. Sakurai, Surf. Sci. Lett. 601 (2007) L136.